

Cosmic Ray Induced Neutron Production in a Lead Target

Haichuan Cao and David Koltick
Department of Physics and Astronomy
525 Northwestern Ave.,
West Lafayette, Indiana USA, 47907
(Dated: January 23, 2024)

Underground experiments searching for rare events, such as interactions from dark matter, need to exhibit background as low as possible. One source of background is from cosmic ray muons and muon-induced neutron production. Presently these background are not fully understood. In this study Geant4 is used to model cosmic ray muon induced neutron multiplicity production and compare the modeling with data collected using an ^3He instrumented Pb-target detector system. The neutron event multiplicity production is taken from the 2002 NMDS-II data sets, consisting of 6504 hrs collected at 583 m.w.e. and 1440 hrs, with the identical detector system, collected at 1166 m.w.e.. The detector consists of a 30 cm cube Pb-target surrounded by 60 ^3He tubes. The single particle detection efficiency is $23.2\% \pm 1.2\%$ calibrated using a ^{252}Cf neutron source. The highest neutron multiplicity event, observed at 583 m.w.e. was 54 observed neutrons corresponding to ~ 233 produced neutrons. The neutron multiplicity, n , distributions fit well a 2-parameter power law fit, $k \times n^{-p}$. For the Monte Carlo simulations at both depths and the data collected at both depths, all are consistent with a single slope parameter p . For the simulation at 583 m.w.e., $p=2.37 \pm 0.01$ and for the data collected at 583 m.w.e., $p=2.36 \pm 0.10$. At 1166 m.w.e., $p=2.31 \pm 0.01$ for the simulation, and for the data with only 6 detected events above multiplicity 5, $p=2.50 \pm 0.35$ predicted using a Maximum Likelihood Estimation method. At both depths, the power law amplitudes of the Geant4 simulations differ by a factor of 2 larger than the data sets. However, the disagreement is within the estimated systematic error of the simulations.

I. INTRODUCTION

Experiments searching for rare events, such as interactions from dark matter, need to exhibit radioactive backgrounds as low as possible. Methods to reduce such backgrounds include the selection of radio-pure materials for building components [1], and placing the experiment deep-underground [1]. Even so, some backgrounds are not avoidable, the most critical of which is background from muon-induced neutrons. These can either generate prompt signals in detectors or produce long lived radioactive isotopes by capture or inelastic scattering reactions. The subsequent decay of the resulting isotopes can lead to significant backgrounds in the detectors if the correlation to the corresponding muon is lost [2]. To shield detectors from the radioactivity experimental components as well as from the surrounding environment, high-Z materials, such as lead, are often selected. Being located close to the sensitive volume such shielding is a source of muon-induced neutrons.

Furthermore, new physics processes initiated by cosmic ray or dark matter-matter interactions may be observable through excess production of high multiplicity neutron production in nuclear targets [3]. For high energy particles, an elemental high mass number solid detector, can be thought of in a manner similar to a solid state detector to γ -rays, except the band gap is of order ~ 10 MeV.

In both cases, whether to improve an understanding of radioactive backgrounds or as a new physics direct search method, further understanding of muon-induced neutron backgrounds is crucial in the search for BSM physics.

To this end, we have analyzed the data collected by the NMDS-II detector, containing 305 kg of Pb, at two

depths, 583 m.w.e. (meters water equivalent) and 1166 m.w.e., located at the Center for Underground Physics in Pyhasälmä(CUPP). The CUPP Underground Laboratory extends down to 1440 m (rock), within the Pyhasälmä zinc, copper and pyrite mine complex in central Finland. Pyhasälmä is the deepest metal mine in Europe[4].

At the experiment's depths neutrino to muon conversion interactions are $\sim 10^{-6}$ below the muon rates[5]. The only source of multiple neutron production then is directly by muon induced production or by particles associated with muon induced showers in the surrounding rock. To set the energy scale, a single ~ 30 TeV muon is expected to pass through the detector in the collected data sets. The data sets record single events producing up to ~ 233 neutrons.

For the 583 m.w.e. (220m rock) data, measurements were collected from February 28th 2002 to February 9th 2003. Taking into account stops for technical reasons, the live acquisition time was 6504 ± 1 hours. In this data set approximately 50% of the events are due to a muon entering through the top and an equal fraction through the sides of the detector. For the 1166 m.w.e. (440m rock) data set collected 1440 ± 1 hours live time, between September 13-th 2001 to January 28-th 2002.

Reported here is a comparison of the two NMDS-II data sets with Geant4 simulations of cosmic ray muon induced neutron production, both directly by muons passing through the detector as well as by interactions in the detector by associated muon induce shower particles produced in the surrounding rock. Separate simulations comparing FLUKA and Geant4 neutron production for muons passing through lead is used to estimate the systematic error of the Geant4 neutron production simula-

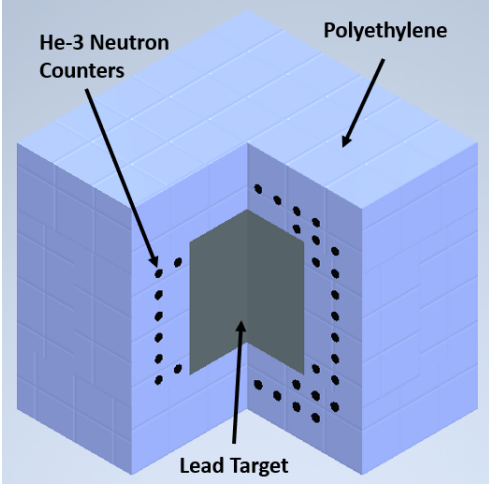


FIG. 1. The NMDS-II detector, consists of a 30 cm cube Pb-target surrounded by 60, ^3He detectors encased in polyethylene. The 60 cm polyethylene cube is composed of 4 side panels, one of which is displayed in cross section on the left side of the cut away.

tions.

II. THE NMDS-II EXPERIMENT

A. Neutron Detection System

The NMDS-II detector is an instrumented 30 cm cube of Pb (305 kg), which serves as the target. The Pb-cube is surrounded by a 60 cm cube polyethylene moderator 15 cm thick, within which 60, ^3He proportional neutron counters, model SNM-18, produced by Maxiums Energy, are encased on all 6-sides, as shown in the Figure 1. The ^3He proportional tubes serve as the neutron multiplicity detection system.

Each counter measures 28.5 cm long and 1.55 cm in diameter filled with a mixture of ^3He (75%) and Ar(25%) at 4 atm pressure and operate in proportional mode at 1400 V. The neutron counters are arranged in 2 cap panels and 4 side panels forming the polyethylene box as shown in the Figure 2. The positions of the ^3He counters were chosen by Monte-Carlo modeling, optimized so that neutron events occurring at any point in the target would be registered with almost the same efficiency.

A single neutron hit triggers the ^3He counter system to record data for 256 μs . Each hit causes the stuck tube to be non-responsive or dead for a period of 10 μs . The neutron half-life in the lead target is 65 μs , resulting in an average of 6.47% of the total neutrons produced to be outside the data collection window.

The two neutron multiplicity data sets collected by the NMDS-II, at 583 m.w.e. and at 1166 m.w.e. are shown in Figure 3.

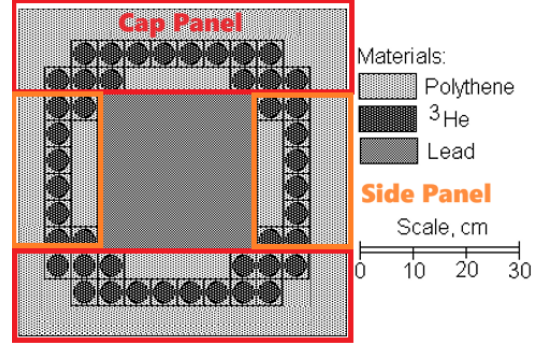


FIG. 2. Cross section through the middle of the NMDS-II detector showing the ^3He neutron counters. The dimensions of the ^3He tubes are not in proportion. The top and bottom cap panels are outlined in red. The side panels are outlined in orange.

B. Experimental Analysis Event Sample

To assure a pure sample of cosmic ray induced neutron events, a minimum of 4 observed neutrons are required to reduce the probability of neutron events produced by natural decays in the rock. At 1166 m.w.e., the observation rate of at least 1 neutron is ~ 0.6 n/s, which includes natural decays and cosmic ray produced neutrons. This rate can be used to set an upper limit on the contribution of non-cosmic ray induced events populating the analysis sample. The probability of 1 neutron in 256 μs , which is the event selection window, is 1.5×10^{-4} . If it is assumed that the number of decay neutrons follows a Poisson distribution, the probability of 4 separate decay neutrons in a 256 μs window is 2.3×10^{-17} , and its contribution to the analysis sample is displayed in Table I.

Because the single independent neutrons contribution is so low, the $n \rightarrow 2n$ process, with threshold at $E_n \sim 7.5\text{MeV}$, and the $n \rightarrow 3n$ process, at $E_n \sim 16\text{MeV}$ are considered. If it is assumed that neutrons from natural decays in the rock have an energy distribution like a ^{252}Cf source, $E^{1/2} \cdot \exp(-E/1.3)$, where E is the neutron energy, the probability for one rock neutron causing an $n \rightarrow 2n$ process is 9.1×10^{-3} or an $n \rightarrow 3n$ process is 1.9×10^{-5} . Again, upper limit contributions of these backgrounds to the cosmic ray sample are displayed in Table I. These estimates have not considered the neutron detection efficiency of the NMDS-II detector system. Doing so would further reduce the probability of observing 4 neutrons from other than cosmic ray sources, significantly.

III. NEUTRON DETECTOR SYSTEM MODELING

The system-wide single neutron detection efficiency was calibrated using a ^{252}Cf source placed at the center of the target and found to be 23.2%. However, the

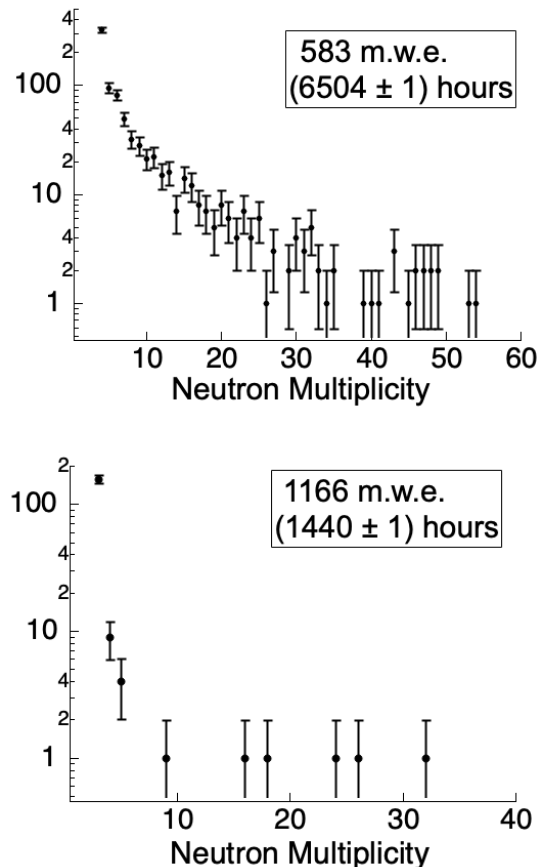


FIG. 3. Observed cosmic ray muon induced neutron multiplicity distributions at 583 m.w.e. (Upper) and at 1166 m.w.e. (Lower), for the observation of 4 or more neutrons.

TABLE I. The upper limit probability of 4 observed neutrons induced by non-cosmic ray sources in the target during the experiment.

	256 μs	1440 hours	6504 hours
4 natural neutron	2.3×10^{-17}	4.7×10^{-7}	2.1×10^{-6}
3 natural neutron, one $n \rightarrow 2n$	5.2×10^{-15}	1.1×10^{-4}	4.8×10^{-4}
2 natural neutron, both $n \rightarrow 2n$	9.9×10^{-13}	2.0×10^{-2}	9.0×10^{-2}
2 natural neutron, one $n \rightarrow 3n$	2.2×10^{-13}	4.4×10^{-3}	2.0×10^{-2}

systems response to ^{252}Cf is not the response to muon induced neutron production because of the difference in their energy spectra. To accurately estimate the detection efficiency of a produced neutron, whether produced in the lead target or surrounding rock, a Geant4 model detector was built matching the geometry of the lead target, the polyethylene thermalizer and the arrangement of ^3He counters.

The ^3He tubes detect neutrons through the reaction



In the Geant4 simulation, when reaction (1) is observed, the corresponding counter is considered to generate a signal or neutron hit, without modeling the complex ion particle motion within the gas and walls of the tubes. If the diameter of the ^3He tube in the simulation is chosen to be 1.55 cm as manufactured, the average neutron efficiency for the ^{252}Cf spectrum is calculated to be $(28.0 \pm 0.1)\%$, which is larger than the measured result. The difference between the simulation predicted efficiency and the measured efficiency is due to the wall effect[6]. The wall effect reduces the detection efficiency because either the proton or the triton or both strike the detector's cathode or the non-sensitive volume at the counters' end, producing a reduced energy pulse, less than the Q in Equation (1). If the energy deposition is below the set threshold, no hit is recorded.

The wall effect, that is the reaction products, $^3\text{He}(n,p)^3\text{H}$ occurring within one mean free path length away from the wall, and the set threshold are then important parameters in calculating the system's neutron detection efficiency. The mean free path length is calculable analytically [7]. Because the ^3He tubes thresholds were set close to Q , the neutron detection efficiency is reduced by a geometric multiplying factor, 82%, due entirely to the Wall Effect. Correcting the ^{252}Cf Monte Carlo calculated calibration efficiency yields $\text{MC}(^{252}\text{Cf}) \times \text{Wall Effect} = 0.28 \times 0.82 \approx 0.23$, in agreement with the measured ^{252}Cf result.

Based on these results, the method used to calculate the neutron detection efficiency was to assume a reduced active ^3He diameter set to 1.33 cm and record as a hit any observation of reaction (1). In order to keep the amount of polyethylene the same, the diameter of the tube is kept at 1.55 cm, but the tube has an empty gap to account for the wall effect and threshold setting.

IV. MUON PROPAGATION TO DEPTH

A. Muon Shower Equilibrium

Cosmic ray muons are capable of penetrating to significant depths underground. At depth, these muon produce a myriad of particles, including photons, electrons, and hadrons. Other cosmic ray particles and those produced as the muon passes through the rock can travel only a short distance, $\sim 2\text{m}$, in the rock. This short path length allows a simplification of the neutron production modeling because the full simulation does not need to start at sea level, but only a few meters above the detectors laboratory hall.

To show this, muons with energy between 100 GeV to 10 TeV are propagated through rock having density $2.85\text{g}/\text{cm}^3$ to find the path length after which the muon induced showers come into equilibrium. The reported observables are in the transverse plane to the muon's initial momentum as a function of the distance from the muon's entry into a 10 m thick rock layer.

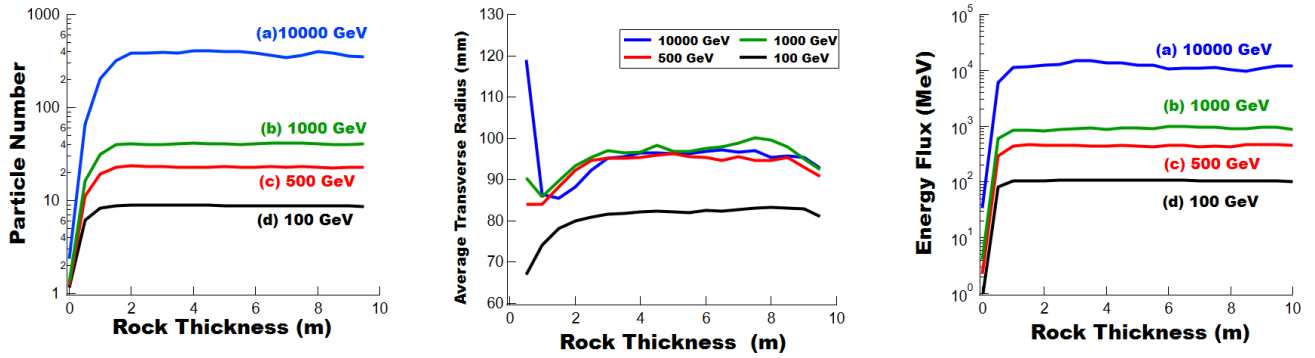


FIG. 4. Simulated, averaged secondary particle flux (left), averaged secondary particle transverse radius (middle) and averaged secondary energy flux (right) passing through transverse planes as a function of muon path length. The averaged secondary flux comes into equilibrium in ~ 2 m independent of muon energy.

Figure 4 shows the results of the Geant4 simulation; (left) shows the averaged number of particles produced; (middle) shows the averaged transverse radial component of secondary particle production. In this case the distribution is not zero at zero thickness. This effect occurs due to energy back-scatter from rock deeper along the muon's path. Figure 4 (right) is the averaged secondary energy flux. All the observables are evaluated on transverse planes to the muon's path. For all distributions, an equilibrium state is achieved within ~ 2 m of rock, independent of muon energy.

While secondary particle production quickly comes into equilibrium there is a concern that secondary muons may have a longer attenuation length than the equilibrium length of the dominating hadronic and electromagnetic components causing an additional muon flux on the Pb-target beyond the sea level component propagated to depth. If a 2.5 GeV cutoff is used, equivalent to the minimum ionizing dE/dx energy loss of a muon passing through 4m of rock, it is found that secondary muons produced by primary muons with 100 GeV, 1 TeV, and 10 TeV, having a path length greater than 4m is less than 10^{-5} , 10^{-4} , 10^{-3} , allowing this secondary source of neutron production in the Pb-target to be neglected.

From these distributions it is concluded to start the full muon shower simulation in a horizontal plane 4m above the detector's cavern hall captures the effects of secondary particle production due to the entire mines over burden, their contribution to neutron production outside the target, and their interactions with the lead target.

B. Muon Propagation from Sea Level to Depth

To correctly model the correlated angular and energy distribution of muons at depth a propagation model must be used starting with the known correlated distributions at sea level. No at depth experimental or analytical correlated distributions are available. However, the validity

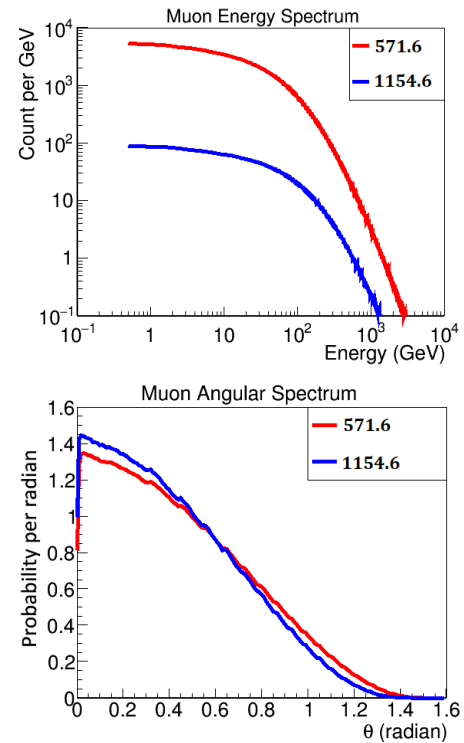


FIG. 5. Cosmic ray muon energy and angular distributions at 571.6 mwe(6504 hr) and 1154.6 mwe(1440 hr). The energy spectra are normalized to the muon number passing through the target top during the data collection period. The mean muon energy for 571.6 m.w.e. is 95.6 GeV and for 1154.6 m.w.e. is 158.7 GeV. The total muon induced event number during the experiment at 571.6 m.w.e. is ~ 36 times that collected at 1154.6 m.w.e.. The two angular spectra are normalized to 1.

of the Geant4 propagation model can be checked, using Miyake's empirical model to compare separately the muon flux density and angular distributions as a function of depth.

The correlated muon distributions at the two NMDS-

II experimental depths are produced by starting with the well-measured energy-angular correlated analytic form of the sea-level cosmic ray muon spectrum [8],

$$\frac{dN_\mu}{dE_\mu d\Omega} \approx \frac{0.14 E_\mu^{-2.7}}{cm^2 s sr GeV} \times \left\{ \frac{1}{1 + \frac{1.1 E_\mu \cos \theta}{115 GeV}} + \frac{0.054}{1 + \frac{1.1 E_\mu \cos \theta}{850 GeV}} \right\}, \quad (2)$$

and propagating individual muons to depth.

Formula (2) is valid when muon decay is negligible ($E_\mu > 100/\cos \theta$ GeV) and the curvature of the Earth can be neglected ($\theta < 70^\circ$). Fortunately, the two limitations do not influence the muon spectrum at 583 m.w.e and 1166 m.w.e underground. As is discussed in Appendix A, muons not suitable for formula (2) will not pass through the thick 583 m.w.e. rock layer.

In the Geant4 model, muons are scattered in the rock, lose energy, create shower particles, and can suffer catastrophic energy loss. The muons are propagated from sea level to 4 m above the laboratory. Only muons are tracked to save simulation time. Shower particles are not tracked once generated. Finally, at depth, the muon's new energy (E'), and angles (θ' and ϕ') are recorded, having the required energy-angular correlation. The generated underground energy and angular spectra are shown in Figure 5. To set the scale for illustration, these energy distributions have been normalized to the number of muons passing through the 30 cm x 30 cm top of the lead target, integrated over the observation time of each data set. Figure 6 shows the Geant4 calculated muon energy flux density at depth as a function of angle for the two locations of the detector 4m above the detector halls.

C. Geant4 and Miyake Formula Comparison

The underground intensity of muons can be calculated with the widely used empirical formula of Miyake. At intermediate depths (100 m.w.e. to 4000 m.w.e.), the Miyake formula is given by [9]

$$I(X) = \frac{A}{X + 400} (X + 10)^{-1.53} e^{-8.0 \times 10^{-4} X}, \quad (3)$$

where, **A** is the only free parameter and **X** is in m.w.e.. **A** was found by fitting measurements made at the Pyhasäalmi mine above and below the experiment[10]. The flux density measurements are presented in Appendix B. The fit returned $A = (2.97 \pm 0.114) \times 10^6$ (m.w.e) $m^{-2} s^{-1}$.

The muon cosmic ray flux density generated by the Geant4 Model and predicted by Miyake's formula are compared as a function of depth in Figure 7. The average difference is 5.8% over the range, 500 m.w.e. to 1200

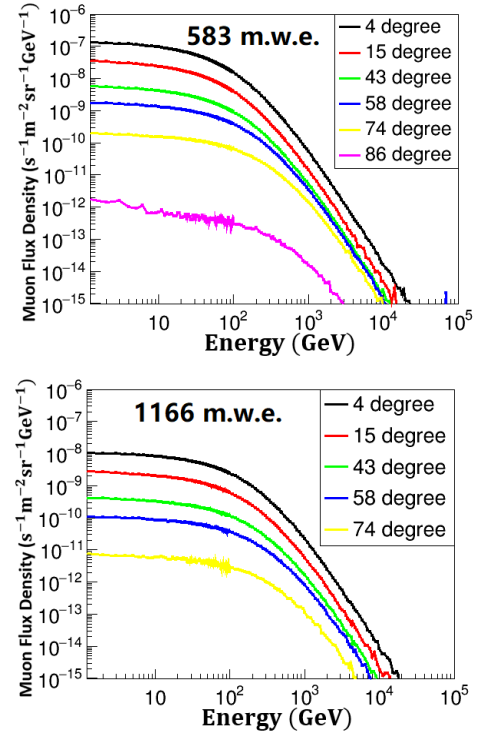


FIG. 6. Muon flux density as a function of angle and incident energy at the experimental depths.

TABLE II. Comparison of the Geant4 and Miiyake single parameter fitted Underground muon density, 4m rock above the experimental caverns.

Depth (m.w.e.)	Miyake Fitting muon s ⁻¹ m ⁻²	Geant4 Simulation muon s ⁻¹ m ⁻²
571.6	0.114	0.123
1154.6	0.0154	0.0148

m.w.e.. The muon flux normalization 4 m rock above the experimental cavities are compared in Table II.

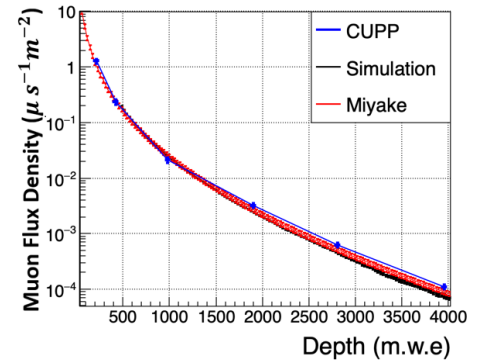


FIG. 7. Muon flux density as a function of depth comparison of CUPP data points(blue), Geant4(black), and Miyake fitted CUPP data(red).

The muon angular distribution formula of Miyake [9]

is given by,

$$I(X, \theta) = I(X, 0^\circ) \cos^{1.53}(\theta) e^{-8.0 \times 10^{-4} X (\sec(\theta) - 1)} \quad (4)$$

where $I(X, 0^\circ)$ is the vertical intensity at depth X . The underground muon angular distributions predicted by the Monte Carlo and Miyake's formula are compared at the two experimental depths in Figure 8. At the two experimental locations the averaged rms difference between the two distributions is less than 1%.

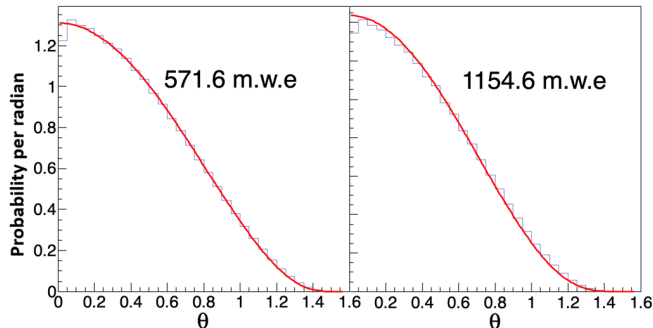


FIG. 8. Comparison of the normalized cosmic ray muon angular distributions 4 m rock above the two experimental halls. Geant4 (blue). Miyake's formula (red).

D. Charge Ratio of the Surface Muons

The final input to the Monte Carlo simulation is the charged muon flux ratio. At depth, for low energy muons, $E_\mu < 1$ GeV, the μ^- cross section with lead is larger than the μ^+ due to attraction with the nucleus. For higher energy muons, $E_\mu > 1$ GeV, the cross sections is nearly charge independent. This effect is displayed in Table III, which shows the average generated neutron number and the reaction probability for muons incident on a 30 cm cube lead target. The reaction probability is the probability of generating at least one neutron.

To correctly take into account the effects of the muon flux charge ratio, the μ^+ and μ^- Geant4 simulation are separately modeled. Only at the end of the complete simulation are they recombined using a single charge ratio value. At 583 m.w.e. depth, muons < 1 GeV require a minimum energy of ~ 150 GeV at sea level to propagate to this level. Likewise at 1166 m.w.e. depth, an energy of ~ 340 GeV is required. Because the μ^+ to μ^- ratio at the surface between 100 GeV and 500 GeV is constant, the value 1.29 ± 0.13 [11] is selected. The estimated charge ratio for higher energy muons is less than the error of the selected value.

TABLE III. The average number of produced neutrons excluding zero neutron production and the probability of generating at least one neutron for a μ^+ or a μ^- incident on a 30 cm cube lead target. From the Geant4 simulation.

		100 MeV	1 GeV	10 GeV
μ^-	$\langle \text{Neutron} \rangle$	4.9	4.7	6.2
	Reaction Probability	0.87	0.0013	0.012
μ^+	$\langle \text{Neutron} \rangle$	1.4	4.3	6.5
	Reaction Probability	0.0034	0.0014	0.011

V. NEUTRON PRODUCTION SIMULATION

A. Geant4 Model

All muon and secondary particle processes in the rock and lead are simulated with Geant4-11.01 using the physics list QGSP-BERT-HP. This list was selected based on its use for LHC experiments. In particular ATLAS and CMS have studied the physics performances of the physics lists and converged on the use of the QGSP-BERT physics list as the most comprehensive and thus the default [12]. Additional simulations for this study included FTFP-BERT-HP, QGSP-BIC-HP and QBBC for possible use in systematic error estimation. However the difference among FTFP-BERT-HP and QGSP-BIC-HP remained smaller than the statistical uncertainties, while there is a 15% deviation in the QBBC list neutron production compared with the other physics lists, making the systematic error estimate using the variation in the physics lists not useful.

B. Model Simulation Universe

The Geant4 simulation begins full shower modeling starting in a horizontal layer 4m above the laboratory hall. Muon generated showers are fully developed allowing the shower particles to interact with the lead target and detector system to generate neutrons.

The model universe is displayed in Figure 9. The NMDS-II detector system, is centered on the floor inside a cavity ($7.5m \times 4m \times 2m$) surrounded by rock. The horizontal thickness of each of the universe's rock side walls is 53 meters. The cavity rests on and is capped by a 4m thick rock floor and roof. Both extend to the outer edges of the side walls forming a rectangular cube. The dimensions were chosen to assure cosmic ray muons with angles from 0 degree to 85.5 degree intersect the top of the universe's roof. The number of slant angle muons passing through the target not covered by this angular range is smaller than 1 over the course of the experiment. The Geant4 simulation inputs are then, (1) the muon flux intensity at depth, (2) the correlated muon energy and muon angular distribution at depth and finally, (3) the cosmic ray muon charge ratio. The full

TABLE IV. Number of cosmic ray muons intersecting the roof of the Geant4 universe during the experimental live times and the number of simulated events at each detector depth.

	583 m.w.e.	1166 m.w.e.
Live Time hrs	6504	1440
Experiment	3.33×10^{10}	9.97×10^8
Simulation	4.58×10^{11}	2.29×10^{11}

simulation starting point is the universe's top surface or roof, $113.5m \times 110m$. The total number of muon events intersecting the universe's roof in the experiments live times are shown in Table IV. The values are found using Eq. 3, Miyake's fit to the experimentally measured [10] muon flux density values, shown in Table II. In order that the simulations have superior statistics compared to the data, more than 10 times the experimental statistics were simulated, also displayed in Table IV.

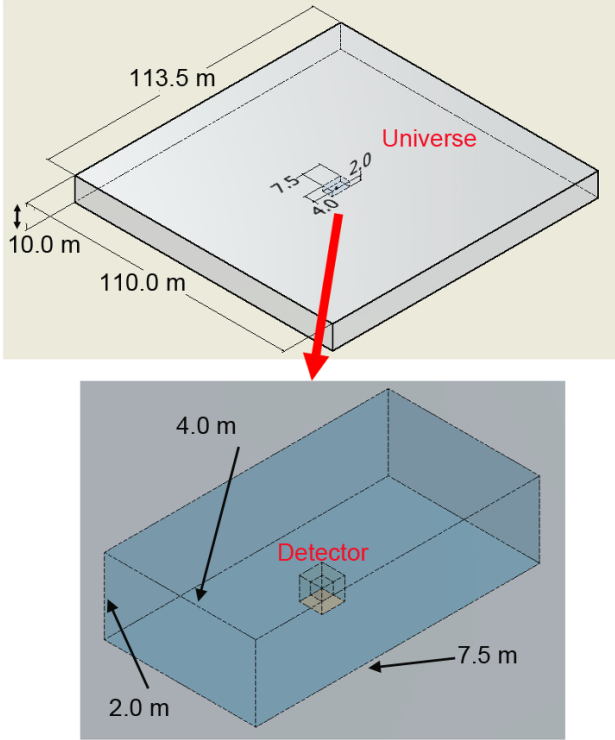


FIG. 9. (Upper) Proportional illustration of the Geant4 Universe, includes the rock layer and (Lower) the laboratory cavern and the detector system, 30 cm Pb-cube inside 60 cm poly-cube sitting centered on the cavern floor.

C. Full Event Simulation Trigger

Because of the large size of the simulation universe and the corresponding low interaction rate of cosmic ray

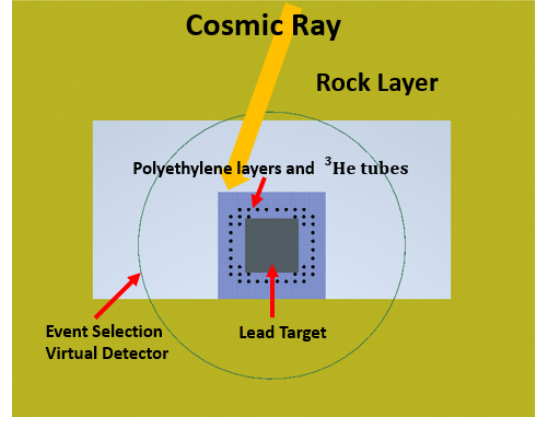


FIG. 10. Illustration of the Geant4 Event Selection Virtual Detector, relative to the ^3He detector system and Pb-target centered on the cavern floor. The dimensions are not in proportion.

showers with the experiment's detectors, a simulation trigger was developed to further reduce the required computational run time. Once the simulation located a muon on the roof of the universe, using its angular parameters the muon track was pointed at the target. The intersection of the muon track with a spherical surface virtual detector was checked and the event was rejected from further consideration if not intersecting the virtual detector. This virtual detector forms a MC trigger for which muons will be fully simulated as they pass through or nearby the target. Figure 10 illustrates the geometry of the model.

For an accurate simulation, it is critical that the event selection virtual detector should be given an appropriate size. Otherwise, some events with neutrons detected will be mis-rejected if the size is too small. However, computing time is roughly proportional to the volume of the virtual detector, or R^3 . Too much computing time will be taken if the event selection virtual detector is too large.

To optimize the radius of the virtual trigger detectors, simulations of the number of detected neutrons as a function of the virtual detector's radius were studied. Figure 11 displays the results. At multiplicity larger than 25 observed neutrons (~ 120 produced neutrons), all the curves for radii between 30 cm to 360 cm are not distinguishable. For these events the distance between the center of the target and the extension line of the muon's initial direction is smaller than 30 cm. When the observed neutron multiplicity is from 14 to 25, the $R=30$ cm curve is separated from other curves. In the same Figure 11, the $R=120$ cm curve is separated from other curves at observed multiplicity equals to 13. At neutron multiplicity equals to 4, the $R=240$ cm curve is separated from the curves $R=300$ cm and $R=360$ cm, while the $R=300$ cm and $R=360$ cm curves are still merged.

Given these distributions, the virtual event trigger detector radius is selected to be $R=300$ cm as neutron multiplicity events lower than 4, are not consider in the sim-

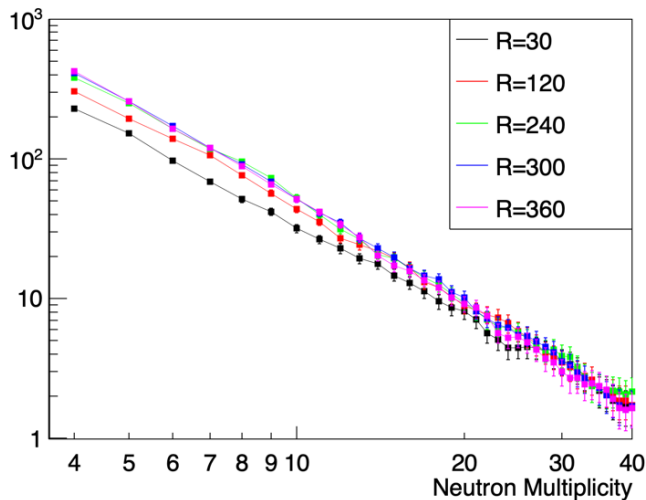


FIG. 11. Log events detected as a function of Log detected neutron multiplicity (n) for selected virtual detector radii. $R=30$ cm separates from others curve at $n = 24$. $R = 120$ cm separates from others at $n=13$, and $R=240$ cm separates at $n=4$. The curve $R=300$ and $R=360$ cm are still merged together at $n=4$.

ulation nor in the experimental measurement.

D. Simulation Statistical Errors Using Bootstrapping

Finally, once a muon is accepted by the virtual trigger for full shower simulation and that event's shower simulation is completed, its neutrons hit times on the ^3He tubes were re-sampled 100 times to get the average response of the NMDS-II He-3 neutron detector system to that event. The statistical errors for the simulations detected neutron multiplicity are estimated using a Bootstrap method[13].

VI. EXPERIMENTAL AND SIMULATION DATA ANALYSIS

A. Power Law χ^2 Fits

The MNDS-II Geant4 simulations results are displayed in Figure 12, for events with observed multiplicity of 4 or more neutrons. The neutron multiplicity distributions are expected to have a power-law distribution. This occurs because the initiating primary hadronic space component, having energy above a few GeV, has a power law intensity fall off, $E^{-\gamma}$ with $\gamma \sim 2.7$ [14]. Because of this, the secondary high energy pion and produced daughter muons have energy intensity fall offs with a similar γ value [15]. As shown in Eq. 2, again the underground muon energy intensity falls off with a similar

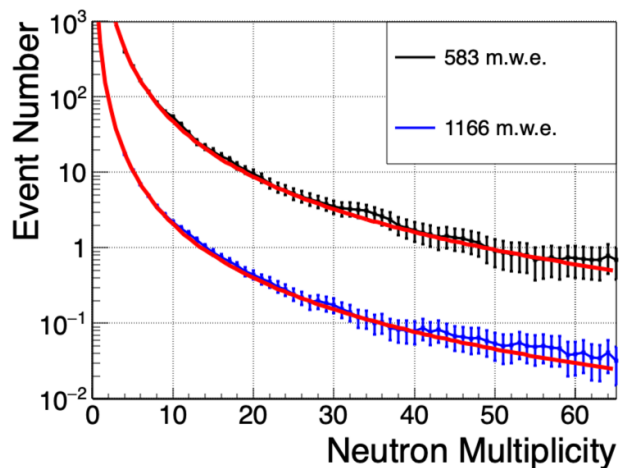


FIG. 12. Comparison of the simulated observed neutron multiplicity distributions with a two parameter power law fit at 583 m.w.e. and at 1166 m.w.e..

γ value. From this the muon induced energy deposited in the Pb-target should have a power law fall off. And finally, because the average number of neutrons produced is roughly proportional to the energy deposited, again the neutron multiplicity is expected to have a power law fall off.

This reasoning is confirmed in Figure 12 displaying the two parameter power law fits, $y = k \times n^{-p}$ to the simulations of the neutron multiplicity distributions. Where k is the amplitude parameter, n is the neutron multiplicity and p is the power law exponent of n .

The results are $\chi^2/\text{DoF} = 1.24$ for the 583 m.w.e. simulation and $\chi^2/\text{DoF} = 1.24$ for the 1166 m.w.e. simulation. Both fits have 60 degrees of freedom. The fitting parameters are displayed in Table V. The same power law parameter value is found in solar neutron emissivity [16].

The experimental data at 583 m.w.e. is compared to its power law fit in the Figure 13 and its parameters are displayed in Table V. In fitting, a multiplicative 5.6% systematic error at each point was included and placed in quadrature with the statistical error. The additional error is due to deterioration of the ^3He tube over the course of data collection. As was the case with the simulation, the data also fits well to a power law yielding $\chi^2/\text{DoF} = 0.76$ for 55 degrees of freedom.

B. Power Law Maximum Likelihood Fit

For the data at 1166 m.w.e. a Maximum Likelihood Estimation (MLE) method is used to measure the power law parameters because there are only 6 points with multiplicity above 5 observed neutrons in the data set. The measurement is made for events whose neutron multiplicity is equal to or larger than 4. In this case the multiplicity probability distribution is $D = A \times n^{-p}$

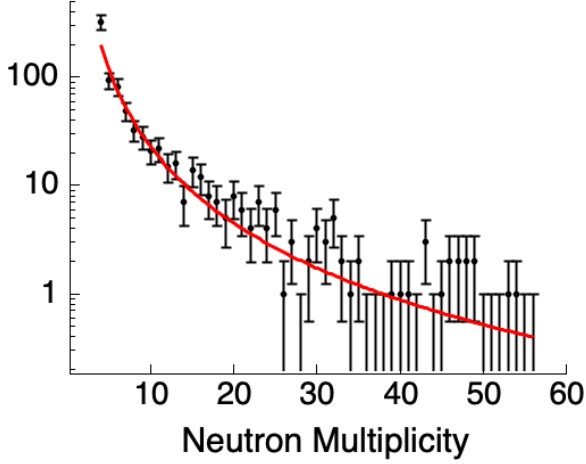


FIG. 13. Experimental data neutron multiplicity distribution at 583 m.w.e. fit with a 2 parameter power law function. Bins with zero counts were fit with an error of 1.

TABLE V. Geant4 simulation and NMDS-II data, neutron multiplicity distribution power law function, $k \times n^{-p}$, fit parameters. The fits are over the range [4,60] observed neutrons. All p parameters can be compared. k values are dependent on the data collection time and are to be compared only at the same depth.

Depth (m.w.e.)	Time (hour)		p	k (10^3)	χ^2 per DoF
583	6504	Geant	2.37 ± 0.01	11.6 ± 2.8	1.24
		Exper	2.36 ± 0.10	5.2 ± 1.2	0.76
1166	1440	Geant	2.31 ± 0.01	0.44 ± 0.11	1.24
		Exper	2.50 ± 0.35	$0.19 \pm 0.17 / - 0.10$	0.76

($n \geq 4$) normalized to one, making the k-parameter or amplitude parameter p-dependent. The one parameter fit then yields $p=2.50$ with an only slightly asymmetric Gaussian shaped Likelihood distribution having $\sigma_{RMS} = 0.35$. From this $p = 2.50 \pm 0.35$. The variation in k is then calculated from the variation in p and is displayed in Table V.

All the fitting results are summarized in Table V.

VII. DATA AND SIMULATION COMPARISON

A. Statistical Error Comparison

The comparison between the NMDS-II data and Geant4 simulation for 583 m.w.e. and 1166 m.w.e. are shown in Figure 14. Comparing the fit parameter results in Table V shows that the power law parameter p values at both depths and for the data and simulation are in excellent agreement. However, the k or amplitude

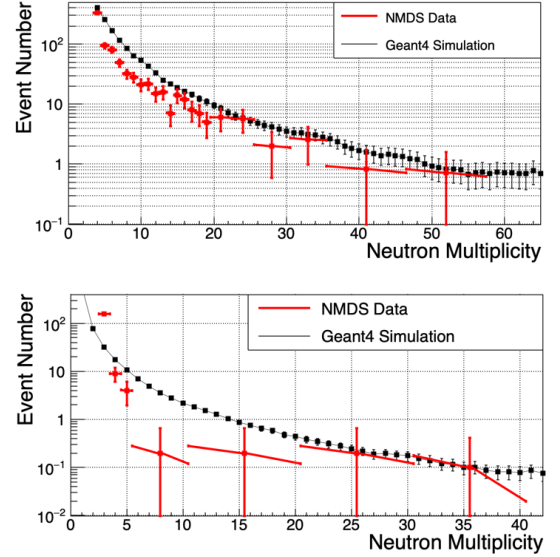


FIG. 14. Comparison of the NMDS-II (Red) neutron multiplicity distributions to the normalized Geant4 simulation (black); (Upper) normalized to 6504 hours of data collection at 583 m.w.e. and (Lower) 1440 hours of data collection at 1166 m.w.e.

parameter, are in disagreement. The k parameter can only be compared between simulation and data at the same depth. k depends on the number of hours of data collection and the muon flux. The Geant4 model yields ~ 2 times as many events as the data at 583 m.w.e., and ~ 4 times the number of events at 1166 m.w.e.. Because a power law function is scale invariant in the power p, this difference can be accounted for by a scale shift in the simulated mean neutron multiplicity of 35% at 583 m.w.e. and 82% at 1166 m.w.e..

These same disagreements are found in data collected at the Boulby Underground Laboratory in UK [17] and Tübingen Shallow Underground Laboratory in Germany [18]. In the Boulby experiment, there was a 0.82 m^3 liquid scintillator at a depth of 1070 m, or 2850 m.w.e.. Their Geant4 model(8.2) gave an average neutron per muon 1.8 times higher than the observed value [17], yielding a k value ~ 4.2 times higher than the observed.

To make a full comparison the systematic errors in the experimental data and simulation must be taken into account.

B. Experimental Systematic Errors

The experimental systematic errors are displayed in Table VI. In order, the Pyhasälmä(CUPP) mine measurement for the cosmic ray flux normalization is taken from Reference [10], stated to be 10%. The error in the rock over burden thickness is estimated to be $\sim 20 \text{ m.w.e.}$. This over burden error is converted to a change in the cosmic flux calculated using the Miyake formula Eq. 3

to be 9.0%.

The efficiency of the ^3He neutron detection system is $(23.2 \pm 1.4)\%$ estimated by the V. G. Khlopin Radium Institute's group [19]. This error causes a scale shift in the simulated observed neutron number. The fit p-parameter in the simulation is used to estimate the shift. In addition, there is a 1.2% efficiency decrease for the ^3He tubes caused by the degradation of the tubes over the course of the measurements. This systematic error causes a scaling effect in the data and was included in the data fitting by increasing each data points error, as was discussed, so is not included again here. Finally, the error in the experimental live time is negligible compared with cosmic ray flux error and depth error, so is dropped.

These experimental errors, added in quadrature, result in a total systematic error of only $\sim 20\%$ which does not significantly improve the comparison between the data and the simulations. Thus, the experimental systematic errors can not account for the difference between the data and the simulation.

The summary of systematic errors in the NMDS-II experiment is shown in the Table VI.

C. Error in the Geant4 Model

To estimate the errors in the Geant4 neutron production modeling, a separate simulation of muon induced neutron production is performed comparing Geant4 and FLUKA. In the study, a muon with fixed initial energy is incident normal to a 30 cm-thick, infinity large lead sheet. The number of neutrons produced are then recorded and averaged over the event sample. The Geant4 and FLUKA simulated neutron production as a function of muon energy is shown in Figure 15 (Upper). In Geant4, muons produce more neutrons than in FLUKA. The production difference increases as a function of muon energy which is clearly seen in the ratio $R = \text{Geant4}/\text{FLUKA}$ displayed as a function of incident muon energy in Figure 15 (Lower). If the difference between the two Monte Carlo simulations is taken as the systematic error in the Geant4 simulation, then this systematic error in produced neutron number results in a scaling error. Due to the scaling invariance of the power law function index, the scaling of k is calculated using the average muon energy incident on the Pb-target at each depth. From the Geant4 cosmic ray muon simulations the muon mean energy at 583 m.w.e. is ~ 95 GeV, with corresponding ratio, $R = 1.29$. The muon mean energy at 1166 m.w.e. is ~ 160 GeV, with corresponding ratio $R = 1.39$. The neutron number scaling factor S is then calculated,

$$S = 1 - R^{-p}, \quad (5)$$

and the resulting errors are displayed in Table VI.

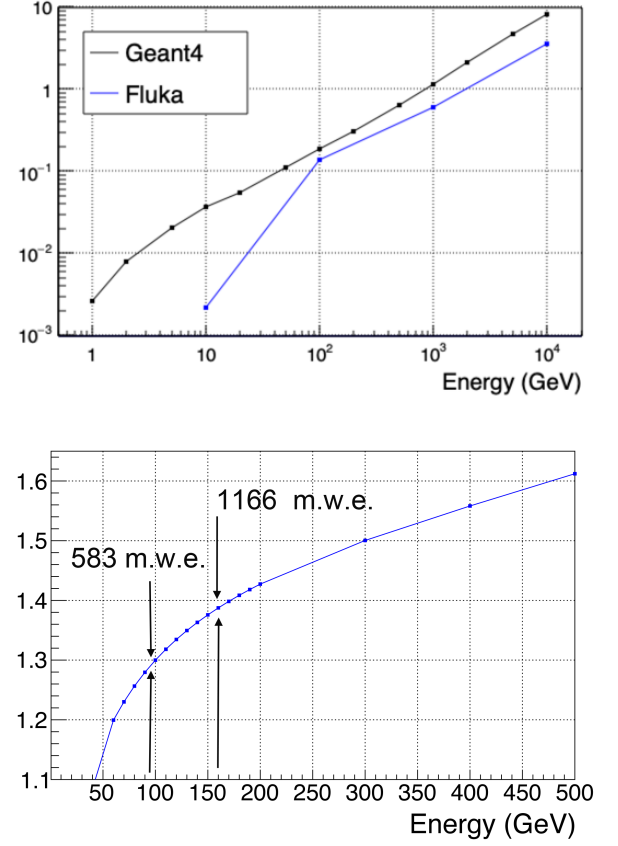


FIG. 15. (Upper) Average number of neutrons produced as a function of incident muon energy from Geant4 and FLUKA. (Lower) Average neutron number ratio, Geant4/FLUKA as a function of muon energy. Muon mean energy at 583 m.w.e. is ~ 95 GeV, with corresponding ratio 1.29. Muon mean energy at 1166 m.w.e. is ~ 160 GeV, with corresponding ratio 1.39.

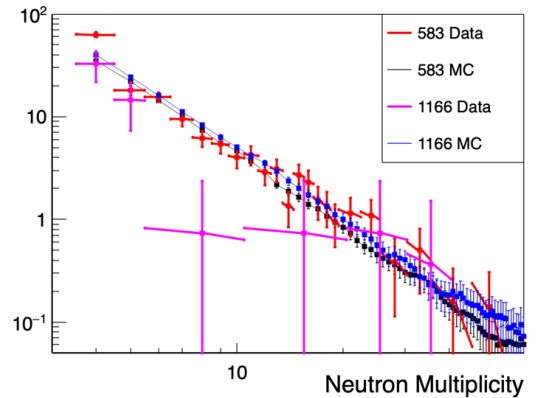


FIG. 16. Amplitude independent comparison of the simulations and experimental neutron multiplicity distributions at both depths. Each curve is fit using $k \times n^{-p}$, however k is shifted to 1000, an arbitrary number, for all distributions for comparison of the power law slope parameter p-values.

D. Comparison Including all Errors

In Table V and displayed in Figure 16 the neutron multiplicity power law parameter p for both the simulation and the data are in good agreement and give good fits to a power law as is expected due to the power law spectrum of the initiating hadronic space component. Errors due to cosmic ray flux intensity, lab depth and ^3He tube efficiency, shown in Table VI do not effect the power law index due to its scaling invariance. These errors cause only an overall normalization motion or amplitude motion in the k -parameter. Likewise, in the simulation, these same errors produce an error only in the k value. In addition any error in Geant4 neutron generation, again displayed in Table VI, produces no change in the power law index, the p -parameter, due to its scale invariance. From this, taking the p -values shown in Table V and forming a ratio between the data and the simulation at a given depth, does not require the inclusion of the systematic errors as they divide out. The resulting comparison at 583 m.w.e. is 1.00 ± 0.04 and at 1166 m.w.e. is 1.08 ± 0.15 .

As discussed, comparing the amplitude parameters, shown in Table V of the simulation and data yeilds a disagreement. The experimental systematic errors can not account for this disagreement. However, assuming the difference between the Geant4 and FLUKA simulations are a measure of their systematic error, Table VII shows that the ratio $\text{Ratio} = \text{Geant4}/\text{data} - 1$ is within 1-standard deviation agreement.

The large size of the systematic error in the simulated neutron production, also shown in Figure 15, indicates that the simulations are poor indicators of the amplitude of muon induced neutron production, making the measured NMS-II neutron multiplicity data critical input to normalizing cosmic ray induced neutron production at depth.

VIII. CONCLUSION

The GEANT4 prediction and the observed data neutron event multiplicity distributions have matching power law shapes $k \times n^{-p}$. The neutron multiplicity production amplitude for the experimental data and simulation are not in agreement and can not be explained by the systematic error in the experimental measurement. Because of this disagreement the simulation does not allow direct prediction of the expected event counts. However, the power law exponent or index values from both simulations and from both experimental data sets are in excellent agreement.

ACKNOWLEDGEMENTS

The authors thank Dr. Thomas Ward from TechSource, Inc for providing the NMDS-II experimental data sets and many insightful discussions, and Alex Barzilov,

TABLE VI. Systematic errors in the data and Geant4 simulations. The detector degradation is included in the data fit.

Errors Effecting p for the NMDS-II Experimental Data		
Error Source	Motion Direction	Systematic Error Propagated to Event Number
1.2 % He-3 Tube Degradation	neutron number	583 : 13.0% 1166 : 12.7%
Errors Effecting k for the Simulation or data		
10% of Cosmic Ray Flux	event number	583: 10% 1166: 10%
20 m.w.e. of Lab Depth	event number	583 : 8.3% 1166: 5.3%
1.4% He-3 Counter Efficiency	neutron number	583: 13.8% 1166 : 13.4%
Geant4 Model	neutron number	583: 45% 1166: 53%
Total Systematic		583: 49% 1166: 56%

TABLE VII. Comparison between Geant4 and collected data values for the amplitude k -parameters. For Geant4, statistical and systematic are displayed separately. For the data sets all systematic and statistical errors have been added in quadrature. Ratio = Geant4/data with all errors added in quadrature.

Depth (m.w.e.)	Geant4 k (10^3)	NMDS-II k (10^3)	Ratio - 1
583	11.6 $\pm 2.8 \pm 5.7$	5.2 ± 1.2	1.2 ± 1.3
1166	0.44 $\pm 0.11 \pm 0.25$	0.19 $+ 0.17/ -0.10$	1.3 $+2.6/ -1.9$

University of Nevada, Las Vegas, for discussions concerning the ^3He -detectors.

This work was funded in part by a grant from the U.S. Department of Energy Office of Nuclear Energy, Contract No. DE-SC0007884; In part by The Department of Physics and Astronomy at Purdue University; and in part by TechSource Inc.

Appendix A: Muon Energy Loss in the Rock

Muons lose energy by ionization and by three radioactive processes; bremsstrahlung, production of electron-position pairs and photonuclear interactions. The muon energy loss was calculated using the form [8],

$$-\frac{dE_\mu}{dX} = a + bE_\mu, \quad (\text{A1})$$

where a is the ionization loss and b is the sum of the three fractional radiative losses. Both are slowly varying

functions of muon energy as shown in Table VIII for standard rock. A second-order polynomial was used to fit a and b , each independently, as a function of $\log_{10}E(\text{GeV})$, yielding the fits values,

$$a = -0.005 * (\log_{10}E)^2 + 0.277 * \log_{10}E + 1.9 \quad (\text{A2})$$

$$b = -0.1775 * (\log_{10}E)^2 + 1.7105 * \log_{10}E + 0.3575 \quad (\text{A3})$$

with only 1 degree of freedom. These values are input in Equation (A1) yielding the point-by-point transformation of the surface energy distribution to one at depth.

TABLE VIII. Average muon range R and energy loss parameters calculated for standard rock[8].

E_μ GeV	R km.w.e	a MeV g^{-1}cm^2	b_{brems}	b_{pair}	b_{nucl}	bE_μ/a	$\delta E \text{ water}$ GeV m^{-1}
			10^{-6} g^{-1}cm^2				
10	0.05	2.17	0.70	0.70	0.50	0.0088	0.219
100	0.41	2.44	1.10	1.53	0.41	0.1246	0.274
1000	2.45	2.68	1.44	2.07	0.41	1.463	0.660
10000	6.09	2.93	1.62	2.27	0.46	14.85	4.643

The validity of this formulation when propagated to NMDS-II depth is supported by a comparison of the formulation and measured data [8], displayed together in Table IX.

TABLE IX. Comprison between the measured range and predicted average muon range using Formula (A1), units in m.w.e..

E_μ	Measured	Predicted	Difference
10	50	48.7	2.6 %
100	410	409	0.24 %
1000	2450	2455	0.21 %
10000	6090	6500	6.3 %

The predicted average muon range in Table IX is obtained by numeral calculations. The muon path in the rock is divided into many small steps. Muon energy loss at each step is then

$$\Delta E = \frac{dE}{dx} \cdot \Delta x \quad (\text{A4})$$

The length of each step was taken to be $\Delta x = 0.01$ m.w.e., and $\frac{dE}{dx}$ is found from Equation (A1). The energy of the muon is changed in each step, so that a in (A2) and b in (A3) are also changed. The predicted muon average range in Table IX is the total length of the muon path in the rock when the energy becomes 0.

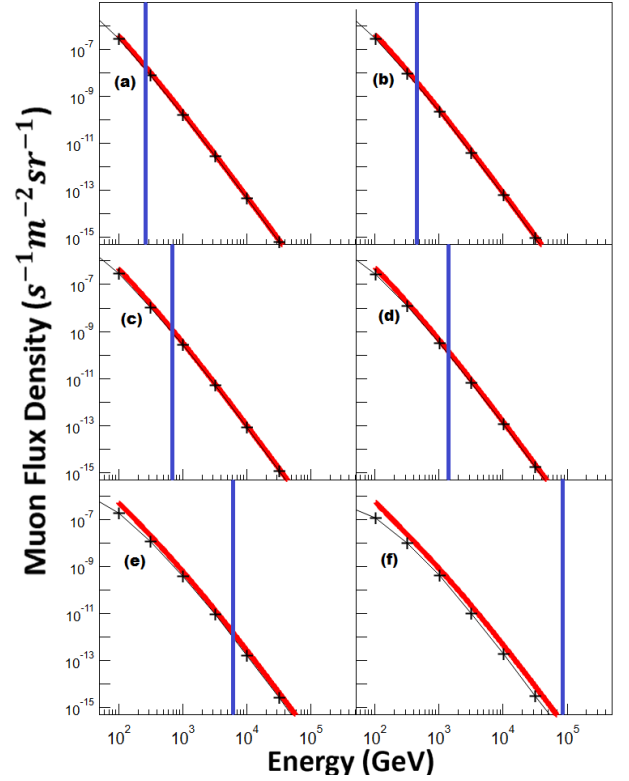


FIG. 17. Sea level cosmic ray muon flux density at a fixed $\cos(\theta)$ (a) 0.6, (b) 0.4, (c) 0.3, (d) 0.2, (e) 0.1, (f) 0.05, comparing Eq. 2 (red line) and the measured data (black points). The comparison is to be made at energies above the vertical bar (blue) indicating the muon energy cut-off or range at the experiments depth of 583 m.w.e..

The slant angle calculated flux and experimental flux is in agreement in the high energy region below the muon cutoff energy or range, shown as a horizontal line (blue) in Figure 17 and listed in Table X. The highest energy events estimated to be observed by the detector is ~ 10 TeV, limiting the slant angle to $\cos(\theta) > 0.05$. The curvature of the Earth was taken into account in these calculations.

Figure 17 shows the cosmic ray muon spectrum predicted by the sea level muon density Formula (2) and from measured data [20] as a function of $\cos\theta$. $\cos\theta$ is chosen as 0.6, 0.4, 0.3, 0.2, 0.1 and 0.05. Only the muons in the part to the right of the blue bar are able to pass through the rock and propagate to 583 m.w.e.. Thus from the Figure 17, the muon flux density predicted by Formula (2) matches well with the experimental data.

Although Formula (2) is only valid when $E_\mu > 100/\cos\theta \text{ GeV}$ $\theta < 70^\circ$, again, muons not in this region will not pass through the thick rock layer to a depth of 583 m.w.e.. From this the underground cosmic ray spectrum can be found by propagating the sea level muon spectra using Formula (2).

TABLE X. Muon energy cutoff at 583 m.w.e as a function of muon slant angle. Eq. 2 is known to be valid for $E_\mu > 100/\cos(\theta)$ GeV [8]. The E_μ cutoff at each incident angle is the energy at which the muon exactly loses all the energy when passing through $583/\cos\theta$ m.w.e.. The curvature of the earth is considered in the calculation of the cutoff energy.

$\cos \theta$	θ	$100/\cos\theta$ GeV	E_μ Cutoff GeV
1.00	0.0°	100	149
0.60	53.1°	167	275
0.40	66.4°	250	463
0.30	72.5°	333	695
0.20	78.5°	500	1330
0.10	84.3°	1000	6045
0.05	87.1°	2000	87800
0.00	90.0°	-	$> 10^6$

Appendix B: CUPP Muon Flux Density as a Function of depth

TABLE XI. Muon Flux Density as a function of depth measured in CUPP [10].

Depth [m.w.e.]	Flux Density [$m^{-2}s^{-1}$]
0	180 ± 20
210	1.3 ± 0.2
420	$(2.3 \pm 0.3) \times 10^{-1}$
980	$(2.1 \pm 0.2) \times 10^{-2}$
1900	$(3.2 \pm 0.3) \times 10^{-3}$
2810	$(6.2 \pm 0.6) \times 10^{-4}$
3960	$(1.1 \pm 0.1) \times 10^{-4}$

-
- [1] V. Kudryavtsev, L. Pandola, and V. Tomasello, Neutron- and muon-induced background in underground physics experiments, *The European Physical Journal A* **36**, 171 (2008).
- [2] A. Best, J. Görres, M. Junker, K.-L. Kratz, M. Laubenstein, A. Long, S. Nisi, K. Smith, and M. Wiescher, Low energy neutron background in deep underground laboratories, *Nuclear Instruments and Methods in Physics Research Section A: Accelerators, Spectrometers, Detectors and Associated Equipment* **812**, 1 (2016).
- [3] T. Ward and W. Traska, Dark matter interpretation of neutron multiplicity anomalies, e-print arXiv:2312.00814v1 [hep-ph] (2023).
- [4] T. Enqvist, J. Peltoniemi, C. Shen, K. T. JamsenT, M. Lehtola, *et al.*, The infrastructure of the centre for underground physics in pyhasalmi mine, Oulu, Finland: University of Oulu (2003).
- [5] M. Crouch, P. Landecker, J. Lathrop, F. Reines, W. Sandie, H. Sobel, H. Coxell, and J. Sellschop, Cosmic-ray muon fluxes deep underground: Intensity vs depth, and the neutrino-induced component, *Physical Review D* **18**, 2239 (1978).
- [6] G. E. Knoll, *Radiation Detection and Measurement* (John Wiley and Sons, Inc., 2000) Chap. 14, pp. 518–519.
- [7] S. Shalev, Z. Fishelson, and J. Cuttler, The wall effect in the counters, *Nuclear Instruments and Methods* **71**, 292 (1969).
- [8] S. W. J.J. Beatty, J. Matthews, Review of particle physics - cosmic rays, *Progress of Theoretical and Experimental Physics* **2019**, 083C01 (2019).
- [9] P. KF, *Cosmic rays at Earth: researcher's reference manual and data book* (Elsevier, 2001) Chap. 4, pp. 485–486.
- [10] T. Enqvist, A. Mattila, V. Föhr, T. Jämsén, M. Lehtola, J. Narkilahti, J. Joutsenvaara, S. Nurmenniemi, J. Peltoniemi, H. Remes, *et al.*, Measurements of muon flux in the pyhäsalmi underground laboratory, *Nuclear Instruments and Methods in Physics Research Section A: Accelerators, Spectrometers, Detectors and Associated Equipment* **554**, 286 (2005).
- [11] V. Khachatryan, A. M. Sirunyan, A. Tumasyan, W. Adam, T. Bergauer, M. Dragicevic, J. Erö, C. Fabjan, M. Friedl, R. Fruehwirth, *et al.*, Measurement of the charge ratio of atmospheric muons with the cms detector, *Physics Letters B* **692**, 83 (2010).
- [12] A. Kiryunin, H. Oberlack, D. Salihagić, P. Schacht, and P. Strizeneć, Geant4 physics evaluation with testbeam data of the atlas hadronic end-cap calorimeter, *Nuclear Instruments and Methods in Physics Research Section A: Accelerators, Spectrometers, Detectors and Associated Equipment* **560**, 278 (2006).
- [13] R. W. Johnson, An introduction to the bootstrap, *Teaching statistics* **23**, 49 (2001).
- [14] A. Apanasenko, V. Beresovskaya, M. Fujiet, *et al.*, Primary cosmic ray spectra observed by runjob, the runjob collaboration, in *Proc. 26th Int. Cosmic Ray Conf., Salt Lake City*, Vol. 3 (1999) pp. 163–166.
- [15] P. K. Grieder, *Cosmic rays at Earth* (Elsevier, 2001) p. 466.
- [16] E. Chupp, D. Forrest, G. Kanbach, E. Flueckiger, and F. Gollietz, Solar neutron emissivity during the large flare on 1982 june 3, *Astrophys. J.* **318** (1987).
- [17] H. Araújo, J. Blockley, C. Bungau, M. Carson, H. Chagani, E. Daw, B. Edwards, C. Ghag, E. Korolkova, V. Kudryavtsev, *et al.*, Measurements of neutrons produced by high-energy muons at the Boulby underground laboratory, *Astroparticle Physics* **29**, 471 (2008).
- [18] R. Kneißl, A. Caldwell, Q. Du, A. Empl, C. Gooch, X. Liu, B. Majorovits, M. Palermo, and O. Schulz, Muon-induced neutrons in lead and copper at shallow depth, *Astroparticle Physics* **111**, 87 (2019).
- [19] V. R. INSTITUTE, Kri nmids ii (unlv) report to date on dm project february 2005 (2005).
- [20] P. Lipari and T. Stanev, Propagation of multi-teV muons, *Physical Review D* **44**, 3543 (1991).